Robust Optimization of Hypoid Gears with Misalignments

A. Bracci, M. Gabiccini, M. Guiggiani

Dipartimento di Ingegneria Meccanica, Nucleare e della Produzione, Università di Pisa, Italy
E-mail: {andrea.bracci, m.gabiccini, guiggiani}@ing.unipi.it

Keywords: Hypoid gears, contact pattern, optimization.

In this work a new automatic procedure to optimize the contact pattern of a hypoid gear drive under misalignment perturbations is presented. It provides the designer with a systematic tool to perform the robust optimization of a hypoid transmission in a few hours and without requiring deep insight on the enveloping and meshing processes. The presented procedure has been tested on several hypoid drives for aeronautical applications.

1 INTRODUCTION

In the aerospace industry, the demand of ever increasing power-to-weight ratios leads to light-weight designs where the flexibility of the rims and the mounting supports must be accounted for in order to avoid premature failure caused by edge contact. Therefore, in aerospace transmissions the optimization of the contact pattern with misalignments within prescribed boundaries is of paramount importance and it is the very motivation of this work.

Several approaches have been proposed to optimize the contact pattern but only at nominal conditions, that is with fixed misalignments. Optimal machine setting corrections can be directly found through sensitivity analysis [1] or, alternatively, through a pinion ease-off topography identification [2]. These methods usually require a trial-and-error approach and the aid of a skilled operator.

In this work we extend the procedure developed in [3], which aimed at obtaining a "good" contact pattern while avoiding edge contacts, to cope with robustness issues caused by uncertain misalignments. While in [3] the misalignments had fixed values, here they may vary within known ranges, thus making the optimization much more demanding.

The proposed method provides the designer with the following benefits: (i) no particular insight in the enveloping and cutting processes is required; (ii) only high-level specifications on the contact pattern shape is requested; (iii) the typical trial-and-error procedure is avoided; (iv) different sets of machine settings can be selected to obtain the same desired pinion tooth surface.

Taking advantage of the low computational cost of the geometric contact pattern estimation procedure presented in [4], the total computational time of a robust optimization is about four hours on a 1.8 GHz computer, thus dramatically reducing the design time with respect to traditional approaches.

2 HYPOID TOOTH MODEL

In the present work, face-milled hypoid teeth are considered. The cutting/grinding process is performed according to the Gleason face-milling, fixed-setting method. The mathematical model is obtained through the *invariant approach* [5, 6].

2.1 Tooth Surface Sampling

Using the same notation of [6] we denote by $\boldsymbol{p}_g(\xi, \theta, \phi)$ the position vector of a generic point of the family of surfaces with motion parameter ϕ, where ξ and θ are the Gaussian coordinates of the tool surface. Due to the complexity of the enveloping process, the mathematical expression of the

hypoid surface is not available in closed form. For this reason it is typically sampled over a given $n \times m$ grid whose generic point is identified by the two values ξ_i and θ_j ($i = 1, \ldots, n; j = 1, \ldots, m$).

The position vector $\boldsymbol{p}_{ij}$ of a generic sampled point P_{ij} is obtained through the solution of the following system

$$\begin{cases} \boldsymbol{p}_{ij} = \boldsymbol{p}_g(\xi_i, \theta_j, \phi_{ij}) \\ f(\xi_i, \theta_j, \phi_{ij}) = 0 \end{cases} \tag{1}$$

where the last one is the *equation of meshing*.

2.2 B-spline Tooth Surface Interpolation

For practical reasons it is better to deal with a closed form surface. To this end a B-spline interpolation of the sampling points P_{ij} is performed yielding the following benefits:

- an approximate closed form tooth surface is obtained;
- a B-spline surface can be easily implemented since it is recursively defined;
- the B-spline domain $U \in \mathbb{R}^2$ is rectangular and it can be chosen as $[0, 1] \times [0, 1] \subset \mathbb{R}^2$;
- if the original tooth surface is sampled on a sufficiently large number of points, then the B-spline approximation gives an accurate representation of it [4].

2.3 Ease-Off Topography Definition

In the literature the ease-off is commonly defined as the deviation of the pinion and gear from their conjugate surface (see for instance [7]). In this work, for simplicity, the ease-off is defined as the flank surface modification with respect to the basic design.

The ease-off topography can be easily defined by a scalar function $h(u, v; \boldsymbol{c})$ as follows

$$h(u, v; \boldsymbol{c}) = \sum_{k=1}^{N} c_k \Psi_k(u, v) \tag{2}$$

where $\Psi_k(u, v)$ are polynomial basis functions, c_k are given coefficients and N the number of basis functions.

Denoting by $\boldsymbol{s}(u, v)$ the position vector of a generic point on the original B-spline surface, and by $\hat{\boldsymbol{s}}(u, v; \boldsymbol{c})$ the position vector of its corresponding point on the modified surface, the ease-off topography is such that the following relation holds

$$\hat{\boldsymbol{s}}(u, v; \boldsymbol{c}) = \boldsymbol{s}(u, v) + h(u, v; \boldsymbol{c}) \boldsymbol{n}(u, v) \tag{3}$$

where $\boldsymbol{n}(u, v)$ is the inward unit normal vector of the original B-spline surface. The definition (3) implies that a positive ease-off stands for material removal.

3 GEOMETRIC CONTACT PATTERN ESTIMATION

The optimization process presented in this paper (see section 4) involves a very large amount of contact pattern calculations. In order to bound the computational time to an acceptable value, a fast contact pattern estimation procedure is required.

In this section the recently introduced [4] geometric approach to contact pattern estimation is briefly described.

3.1 Tooth Contact Analysis

Denote by $\boldsymbol{s}_{f1}(u_1, v_1, \varphi_1)$ and $\boldsymbol{s}_{f2}(u_2, v_2, \varphi_2)$ the pinion and gear B-spline interpolated surfaces expressed into a fixed reference frame. The two variables φ_1 and φ_2 represent the pinion and gear rotation about their respective axis $\boldsymbol{e}_1$ and $\boldsymbol{e}_2$ as shown in Figure 1. It is worth remarking here that

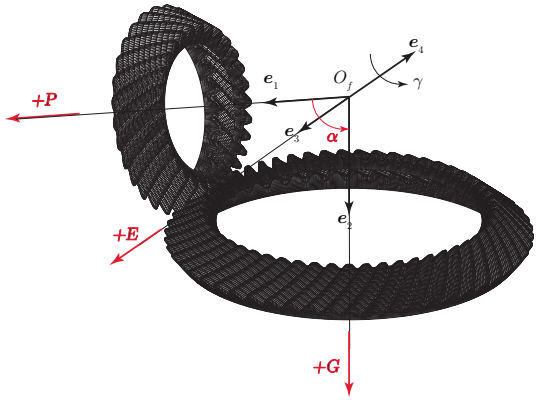

Figure 1: System set up. The assembly error positive directions are red highlighted.

the relative position between the pinion and the gear depends on the *misalignments* E, P, G and α, also known as *assembly errors* and defined as in Figure 1.

Assuming that pinion as the driving member, the meshing condition is given by the solution of the following system for all φ_1:

$$\begin{cases} \boldsymbol{s}_{f1}(u_1, v_1, \varphi_1) = \boldsymbol{s}_{f2}(u_2, v_2, \varphi_2) \\ \boldsymbol{m}_{f1}(u_1, v_1, \varphi_1) = \lambda \boldsymbol{m}_{f2}(u_2, v_2, \varphi_2) \end{cases} \tag{4}$$

where $\boldsymbol{m}_{f1}(u_1, v_1, \varphi_1), \boldsymbol{m}_{f2}(u_2, v_2, \varphi_2)$ are the normal vectors to $\boldsymbol{s}_{f1}(u_1, v_1, \varphi_1), \boldsymbol{s}_{f2}(u_2, v_2, \varphi_2)$, and λ is a scalar value. For a given φ_1, the system (4) consists of six equations in the six unknowns $(u_1, v_1, u_2, v_2, \varphi_2, \lambda)$ and hence it can be solved numerically. The solution of (4) produces then the following functions

$$(u_1(\varphi_1), v_1(\varphi_1), u_2(\varphi_1), v_2(\varphi_1), \varphi_2(\varphi_1), \lambda(\varphi_1)) \tag{5}$$

and it is worthwhile to remark that these take into account the misalignments.

Denoting by N_1 and N_2 the pinion and gear tooth number, the transmission error $\Delta\varphi_2(\varphi_1)$ is defined as follows

$$\Delta\varphi_2(\varphi_1) = \varphi_2(\varphi_1) - \frac{N_1}{N_2}\varphi_1 \tag{6}$$

The graphical representation of (6) is known as *motion graph* and Figure 2 shows a sample of it.

3.2 Instantaneous Contact Area Estimation

In order to estimate the instantaneous contact area *under load*, the so called *rolling-test* is simulated. To this end a virtual uniform *marking compound* is superimposed over the gear surface. The resulting surface is denoted by $\hat{\boldsymbol{s}}_{f2}(u_2, v_2, \varphi_2)$ and it is defined as follows

$$\hat{\boldsymbol{s}}_{f2}(u_2, v_2, \varphi_2) = \boldsymbol{s}_{f2}(u_2, v_2, \varphi_2) + t\, \boldsymbol{n}_{f2}(u_2, v_2, \varphi_2) \tag{7}$$

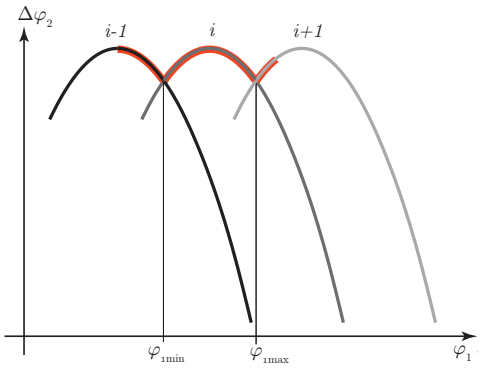

Figure 2: Motion graph of three consecutive tooth pairs. The red highlighted line indicates the range of contact of the i-th tooth pair

where t is the marking compound thickness and $\boldsymbol{n}_{f2}(u_2, v_2, \varphi_2)$ is the unit outward normal to the interpolated gear surface. Then, for each value of the pinion rotation angle φ_1, the following nonlinear system is solved:

$$\boldsymbol{s}_{f1}(u_1, v_1, \varphi_1) = \hat{\boldsymbol{s}}_{f2}(u_2, v_2, \varphi_2(\varphi_1)) \tag{8}$$

A tooth pair composed by a pinion and a gear tooth is considered to be *in contact* if system (8) admits solutions. Since, for a given φ_1, system (8) involves three equations and four unknowns (u_1, v_1, u_2, v_2), then the obtained solution is a spatial curve $\Gamma(\varphi_1)$.

It is important to stress here that the value of $\varphi_2(\varphi_1)$ depends on the tooth pair that, for a given φ_1, produces the largest value of $\Delta\varphi_2$ (unilateral contact): with reference to Figure 2, the i^{th} tooth pair determines the rigid rotation of the two mating members only between $\varphi_{1_{\min}}$ and $\varphi_{1_{\max}}$. However, due to the presence of the marking compound, the i^{th} tooth pair is in contact for a larger range which is highlighted in Figure 2.

3.3 Contact Pattern Estimation

Denoting by $r_i z_i$-domain the cylindrical projection plane with respect to the i-th mating member (see [8], then for each φ_1 the intersection curve $\Gamma(\varphi_1)$ is mapped into $r_1 z_1$ and $r_2 z_2$ thus delimiting a typical elliptically-shaped area. The estimated contact pattern on both members is then given by the convex hull of such areas, as depicted in Figure 3.

The result of the geometric contact pattern estimation procedure strongly depends on the marking compound thickness t. A tuning process is thus required in order to match a reference contact pattern obtained, e.g., with a FEM analysis tool (see [4]). Figure 4 shows the comparison between the output of the commercial software *HypoidFaceMilled* [9] and the result of the geometric contact pattern procedure after tuning the marking compound.

3.4 Perturbed Contact Pattern Estimation

The previous procedure for contact pattern estimation considers only a given set of misalignments, i.e., the so-called *nominal conditions*. Nonetheless, especially in aeronautical applications, the compliance of the transmission components may sensibly affect the relative position between the pinion and the gear in operating conditions. Therefore the misalignments may vary within a bounded

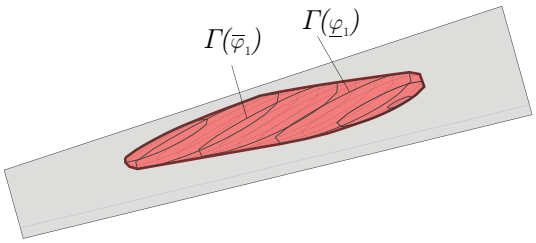

Figure 3: Instantaneous contact areas (thin and dashed lines); estimated contact pattern (red shaded with thick line). The two highlighted areas are obtained with two different values of φ_1.

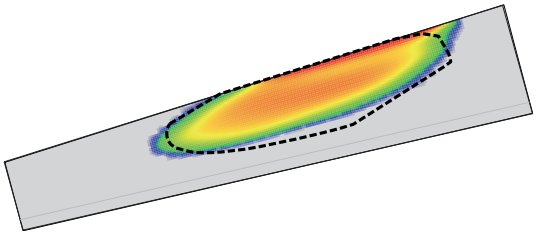

Figure 4: HFM results (shaded); estimated contact pattern (black dashed line).

range as expressed below

$$\begin{aligned} E &\in [E_0 - \Delta_{E_m}, E_0 + \Delta_{E_M}] \\ P &\in [P_0 - \Delta_{P_m}, P_0 + \Delta_{P_M}] \\ G &\in [G_0 - \Delta_{G_m}, G_0 + \Delta_{G_M}] \\ \alpha &\in [\alpha_0 - \Delta_{\alpha_m}, \alpha_0 + \Delta_{\alpha_M}] \end{aligned} \tag{9}$$

where E_0, P_0, G_0, α_0 are the nominal misalignments and $\Delta_{x_m}, \Delta_{x_M}$ identify the lower and upper deviation of the misalignment x. The goal now is to estimate the contact pattern in all the perturbed conditions, and then estimate a precautionary *worst-case* contact pattern. To this end the variation range of each misalignment is divided into a given number of parts N_E, N_P, N_G and N_α and the contact pattern is estimated for all the misalignment combinations. The *worst-case* contact pattern is thus given by the convex envelope of all the estimated contact patterns, as it is shown in Figure 5.

4 CONTACT PATTERN OPTIMIZATION

The goal of the contact pattern optimization is to modify the pinion ease-off topography in order to match a prescribed contact pattern in both nominal and perturbed conditions. The coefficients $\boldsymbol{c}$ that define the ease-off shape (3) are thus unknown and the optimization process seeks for the optimal values of $\boldsymbol{c}$ such that a given objective function $J(\boldsymbol{c})$ is minimized. The optimal solution $\boldsymbol{c}^*$ is thus defined as follows

$$\boldsymbol{c}^* = \arg\min_{\boldsymbol{c}} J(\boldsymbol{c}) \tag{10}$$

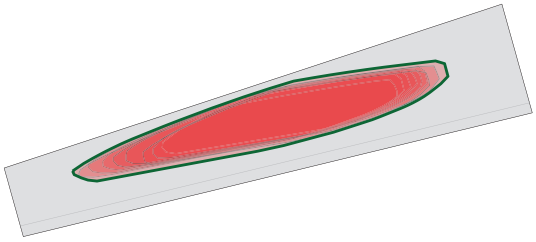

Figure 5: Contact patterns estimated with different misalignments (red shaded with thin black line); perturbed contact pattern (thick green line).

After extensive tests the *Nelder-Mead* simplex minimization algorithm that does not require derivatives, was found suitable for the solution of (10).

4.1 Target Definition

The target contact pattern is established according to the *Design Manual for Bevel Gears* (ANSI-AGMA 2005-D03 [10]): an optimal contact pattern should utilize virtually the total tooth length and should be sufficiently far from the tooth bounds to prevent edge/corner contact situations. A realistic target contact pattern has a typical elliptical shape as the one shown in Figure 6.

4.2 Objective Function Definition

For a given $\boldsymbol{c}$, denote by $A_i(\boldsymbol{c})$ the area of the current contact pattern, and by $A_{I_i}(\boldsymbol{c})$ the intersection area between the target contact pattern and the current one. The objective function $J(\boldsymbol{c})$ to be minimized is defined as follows

$$J(\boldsymbol{c}) = \sum_{i=1}^{2} \left(w_{d_i} d_i(\boldsymbol{c}) + w_{a_i} A_{n_i}(\boldsymbol{c}) + w_{e_i} e_i(\boldsymbol{c}) \right) \tag{11}$$

where

- $i = 1, 2$ stands for the pinion and gear respectively;
- $d_i(\boldsymbol{c})$ is the distance between the centroids of the current and the target contact patterns;
- $A_{n_i}(\boldsymbol{c})$ is the *non-overlap* area defined as

$$A_{n_i}(\boldsymbol{c}) = \frac{A_{t_i} + A_i(\boldsymbol{c}) - 2A_{I_i}(\boldsymbol{c})}{A_{t_i} + A_i(\boldsymbol{c})} \tag{12}$$

  and represented as a shaded area in Figure 6;
- $e_i(\boldsymbol{c})$ is a penalty function that has a large value if the current contact pattern is close to the tooth edge, and zero elsewhere;
- w_{d_i}, w_{a_i} and w_{e_i} are tunable weights.

Therefore the minimization of (11) according to (10) agrees with the above specifications.

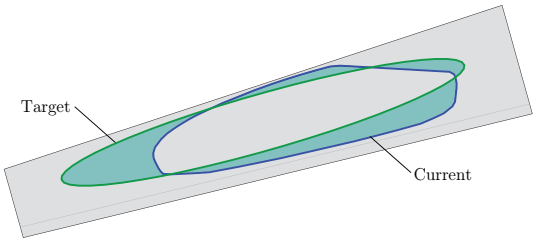

Figure 6: Target contact pattern (green); current contact pattern (blue); non-overlap area (shaded).

4.3 Nominal and Robust Optimization

The goal of the *nominal optimization* is to find the optimal ease-off shape defined by $\boldsymbol{c}^*$ such that the nominal contact pattern (Figure 3) matches the target one. However, in order to check the robustness of the resulting contact pattern a sensitivity analysis must be performed considering the misalignment perturbations.

Extensive simulations have shown that, although the nominal contact pattern matches closely the target one, one or more perturbed contact patterns may show edge contact situations (see section 6). For this reason the misalignment perturbations must be taken into account *during* the optimization process.

The goal of the *robust optimization*, therefore, is to assure that all the perturbed contact patterns (Figure 5) do not present edge contact situations. This kind of optimization, though computationally more demanding than the nominal one, has the following advantages

- the misalignment perturbations are considered during the optimization process;
- edge/corner contact situations of one or more perturbed contact patterns are avoided;
- *a posteriori* sensitivity analysis is not required since robustness is ensured by the optimization process itself.

5 MACHINE SETTINGS IDENTIFICATION

The optimal ease-off obtained through the solution of problem (10) is, until now, a *virtual* surface to be superimposed over the pinion tooth according to (3) in order to match a desired contact pattern. The resulting surface (3) has to be physically realized through an enveloping process.

The goal is then to obtain such surface via machine setting modifications. The *machine settings* are the set of parameters that define the hypoid tooth geometry and contain

- the geometric parameters to define the tool surface;
- the parameters that define the machine kinematics.

This problem is formulated as a *nonlinear least square* minimization (NLS) that involves a chosen subset $\boldsymbol{x}$ of all the machine settings [3, 11].

With $h(u, v; \boldsymbol{c}^*)$, the target surface (3) is sampled over a given grid, yielding a set of target points $\boldsymbol{p}_k$. Then, for a given $\boldsymbol{x}$ the *misfit* $f(\boldsymbol{x})$ between the target and the current surface $\Gamma(\boldsymbol{x})$ is estimated by

$$f(\boldsymbol{x}) = \frac{1}{2}\boldsymbol{h}(\boldsymbol{x})^T\boldsymbol{h}(\boldsymbol{x}) \tag{13}$$

where the generic component $h_k(\boldsymbol{x})$ of the vector $\boldsymbol{h}(\boldsymbol{x})$ represents the distance between $\boldsymbol{p}_k$ and $\Gamma(\boldsymbol{x})$. The machine settings $\boldsymbol{x}^*$ that identify the optimal ease-off are found as

$$\boldsymbol{x}^* = \arg\min_{\boldsymbol{x}} f(\boldsymbol{x}) \tag{14}$$

The solution of (14) is obtained by employing the *Levenberg-Marquardt* algorithm with a *trust region* approach [12] that guarantees convergence to a local minimum, and deals efficiently with ill-conditioned problems.

6 TEST-CASE

The capabilities of the optimization procedure presented in this paper are now demonstrated through a numerical test. The results presented here are obtained with a software package developed by the authors[1]. The full optimization process is composed by the following sequential steps:

- marking compound thickness tuning;
- target contact pattern definition;
- optimization at the design point:
  - nominal ease-off optimization;
  - identification of the nominal-optimal ease-off;
  - robustness analysis;
- robust optimization:
  - robust ease-off optimization;
  - identification of the robust-optimal ease-off;
  - robustness check.

Each of the previous steps is performed with a single function call of the developed software. In addition, the full optimization process may be executed with a single command via a batch procedure. It is worthwhile to remark here that the full optimization process takes only five hours on a 1.8 GHz computer.

6.1 Basic Design

Some basic settings of the considered transmission are collected in Table 1. The contact pattern calculated by HFM at the design point shows an undesirable edge contact on the gear tip. After the marking compound tuning process, the geometric contact pattern procedure detects the same edge contact, as shown in Figure 7. The hypoid drive has therefore to be optimized.

[1]The software has been developed in C++ with more than 60.000 lines of code. Several executable files have been created to perform the full hypoid transmission optimization and analysis.

Pinion tooth number	31
Gear tooth number	50
Shaft angle	105.5 deg
Mean spiral angle	35.0 deg
Pinion hand	RH
Face width	33.0 mm
Outer cone distance	100.36 mm
Pinion torque	504.4 Nm
Nominal misalignments	E_0= 0.245 mm
	P_0= 0.608 mm
	G_0= $-$0.009 mm
	α_0 = $-$0.087 deg

Table 1: Some basic design data of the transmission.

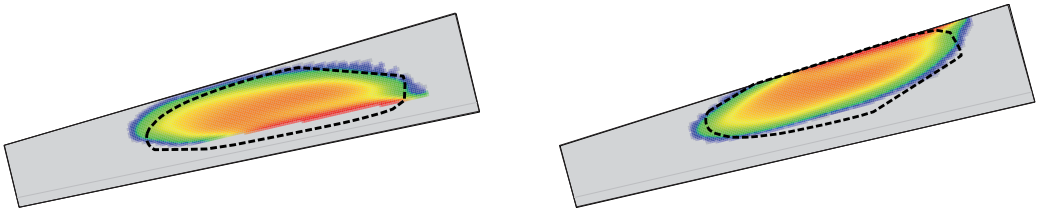

(a) pinion tooth (concave side) (b) gear tooth (convex side)

Figure 7: Basic loaded patterns: (color areas) HFM patterns; (black dashed curves) geometrically estimated.

6.2 Nominal Optimization at the Design Point

The target contact pattern is defined as an ellipse over the two teeth in their rz-domain, as it is shown in Figure 9. The optimal coefficients $\boldsymbol{c}^*$ of the polynomial basis functions that define the ease-off are obtained with about 250 iterations of the Nelder-Mead algorithm, in less than one hour of computational time.

The machine settings identification has been performed using two different sets of parameters: (i) the former (STD) contains 13 parameters that are typically employed by Gleason for tooth topography optimization; (ii) the latter (CUSTOM) contains 14 parameters that are slightly different from the previous ones. Both sets give good results in term of the residual error and the final ease-off obtained with the CUSTOM set is shown in Figure 8. The new machine settings are collected in Table 2, while the obtained contact pattern at the design point is shown in Figure 9.

A robustness analysis is then performed over the nominally-optimized transmission with respect to the following misalignment perturbations:

$$\Delta_{E_m} = \Delta_{E_M} = 0.1, \quad \Delta_{P_m} = \Delta_{P_M} = 0.2, \quad \Delta_{G_m} = \Delta_{G_M} = 0.1 \tag{15}$$

The result of this analysis shows that in some perturbed condition an edge contact situation occurs. This condition is confirmed by the correspondent analysis in HFM as shown in Figure 10. A robust optimization is thus required in this case, since the optimization at the design point does not guarantees no edge contact situation under all the perturbed conditions.

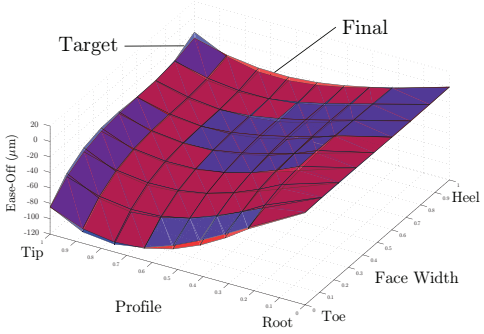

Figure 8: Target ease-off (blue); obtained ease-off (red).

		NOMINAL		ROBUST	
Parameter	BASIC	STD	CUSTOM	STD	CUSTOM
Cutter p. rad. (mm)	79.01	81.56	77.10	82.19	74.57
Blade angle (deg)	17.42	9.97	—	8.67	—
Spherical rad. (mm)	350.89	46.83	117.54	35.77	63.49
Rad. sett. (mm)	72.14	113.23	108.27	90.37	116.55
Blank off. (mm)	−5.08	−27.76	26.15	7.66	36.00
MCTB (mm)	2.71	28.51	27.00	14.62	30.30
Sliding base (mm)	−1.51	−15.82	−14.98	−8.11	−16.82
Cradle angle (deg)	59.73	59.59	58.03	59.82	58.48
Ratio of roll	1.7066	2.7109	2.5791	2.1631	2.5791
2C	0.0226	0.1892	0.3230	0.0667	0.4392
6D	-0.0329	−3.4663	-2.4215	−1.625	-4.2203
24E	0.0	−15.6035	14.2764	1.7878	37.8946
120F	0.0	−409.385	-295.1172	−58.214	-520.366
H_1 (mm/rad)	0.0	—	0.0522	—	-0.00838
H_2 (mm/rad^2)	0.0	—	0.2474	—	0.03669

Table 2: Basic and optimal settings for the contact pattern optimization at the design point and under perturbed conditions.

6.3 Robust Optimization

The robust optimization is then performed considering the same misalignment tolerances (15) and the coefficients of the robust-optimal ease-off are obtained with 300 iterations of the Nelder-Mead algorithm in about four hours of computational time.

The robust-optimal ease-off is then identified with the same two sets of machine parameters that has been used for the nominal optimization. As for the previous case, both sets produce good result in terms of the residual error, and the final ease-off obtained with the CUSTOM set is shown in Figure 11. The resulting machine parameters are collected in Table 2.

As a final step the robustness of the modified transmission is checked: for each misalignment combination the contact pattern estimated via the geometric approach is compared with the contact pattern calculated with HFM. The results of the robustness analysis are shown in Figure 12. quite remarkably in this case no edge contact situations occur thus validating the robust optimization procedure.

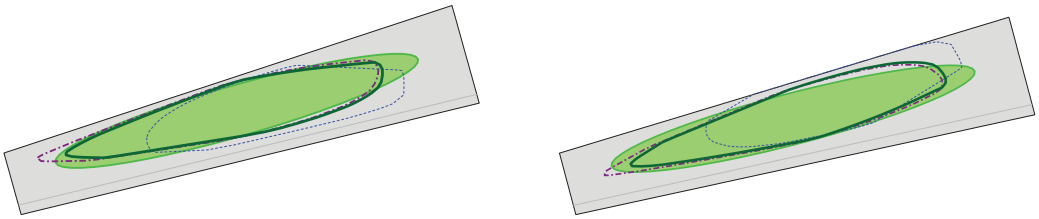

(a) pinion tooth (concave side) (b) gear tooth (convex side)

Figure 9: Contact patterns: basic (blue dashed line); target (green shaded); optimized (purple dash-dotted line); after identification (green solid line).

7 CONCLUSION

In this paper a fully automatic procedure to optimize the contact pattern of a hypoid gear drive under misalignment perturbations has been presented. This procedure does not require a skilled operator and it allows to robustly optimize a hypoid transmission in a few hours.

The systematic nature of the presented methodology allows to address other indices of performance of a hypoid drive, such as the transmission error function, and to deal with the robustness with respect to topography errors.

8 ACKNOWLEDGEMENT

The support of *Avio S.p.A.* is gratefully acknowledged.

References

[1] V. Simon. Optimal tooth modifications in hypoid gears. *ASME Journal of Mechanical Design*, 127:646–655, 2005.

[2] Y.-P. Shih and Z.-H. Fong. Flank modification methodology for face-hobbing hypoid gears based on ease-off topography. *ASME Journal of Mechanical Design*, 129:1294–1302, 2007.

[3] A. Artoni, A. Bracci, M. Gabiccini, and M. Guiggiani. Optimization of the loaded contact pattern in hypoid gears by automatic topography modification. *ASME Journal of Mechanical Design*, 131, January 2009.

[4] A. Bracci, M. Gabiccini, A. Artoni, and M. Guiggiani. Geometric contact pattern estimation for gear drives. *Computer Methods in Applied Mechanics and Engineering*, 198, April 2009.

[5] F. Di Puccio, M. Gabiccini, and M. Guiggiani. Alternative formulation of the theory of gearing. *Mechanism and Machine Theory*, 40(5):613–637, 2005.

[6] F. Di Puccio, M. Gabiccini, and M. Guiggiani. An invariant approach for gear generation with supplemental motions. *Mechanism and Machine Theory*, 42(3):275–295, 2007.

[7] H. J. Stadtfeld. *Handbook of Bevel and Hypoid Gears*. Rochester Institute of Technology, Rochester, 1993.

[8] H. J. Stadtfeld. *Advanced Bevel Gear Technology*. The Gleason Works, Rochester, 2000.

[9] S. Vijayakar. *HypoidFaceMilled*. Advanced Numerical Solutions, Columbus OH, May 2005.

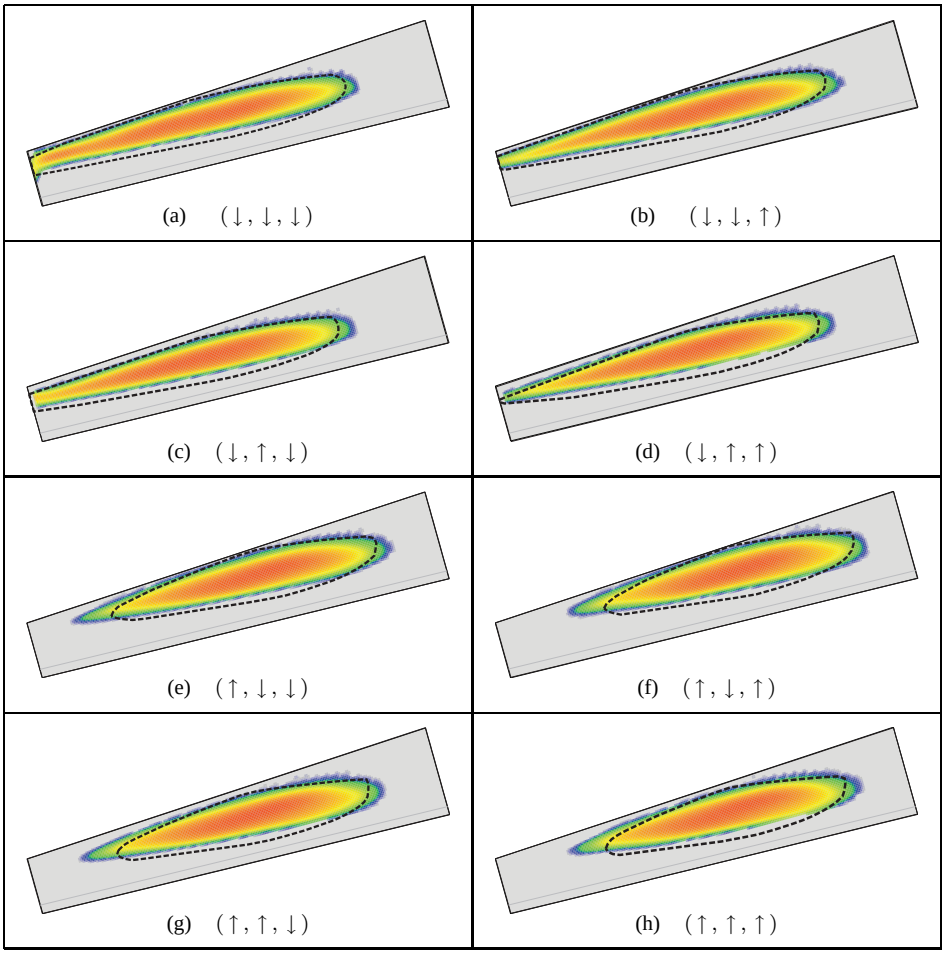

Figure 10: Perturbed contact patterns for different E, P and G and ease-off topography optimized at the design point.

[10] ANSI/AGMA 2005–D03. *Design manual for bevel gears*. ANSI–AGMA, 2005.

[11] A. Artoni, M. Gabiccini, and M. Guiggiani. Synthesis of hypoid gear surface topography by a nonlinear least squares approach. In *IDETC/CIE*, 2007.

[12] J. Nocedal and S. J. Wright. *Numerical Optimization*. Springer Verlag, New York, 1999.

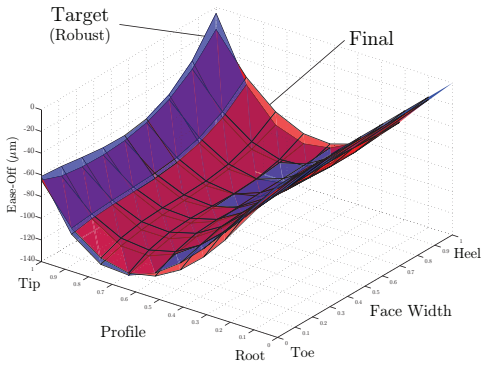

Figure 11: (Blue) Robust target ease-off; (red) obtained ease-off.

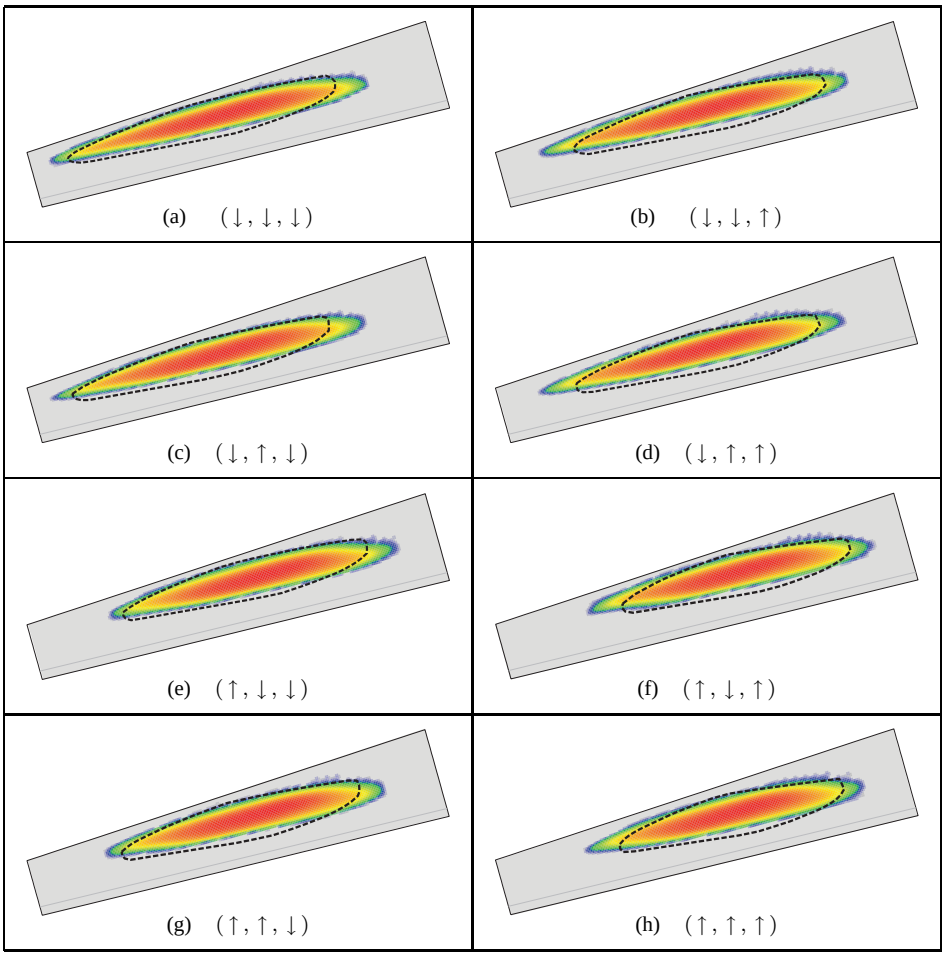

Figure 12: Perturbed contact patterns for different E, P and G and ease-off topography optimized under perturbed conditions.